Usage Report for Fiscal Year 2021

**Project Title:**

# The numerical analysis of oxygen transport in the microcapillary network.

○ **Xiaolong Wang**

**Laboratory at RIKEN:**

**RIKEN Center for Advanced Photonics Image Processing Research Team**

## 1. Background and purpose of the project, relationship of the project with other projects

The steady motion of red blood cells (RBCs) in microtubules is a critical topic in cellular-scale hemodynamics and microfluidic applications. A systematic understanding of this issue is critical for not only understanding the mechanisms of mass transport in microcirculation, but also for a variety of applications in microfluidics, including biomimetic carriers, cell sorting, and high-throughput measurement of cell deformability.

Previous studies have explored the equilibrium condition of erythrocytes in microchannels experimentally and numerically, and found that there exist different equilibrium states in the microchannel, including "tumbling", "parachutes" and "slippers". Numerous variables influence the RBCs' equilibrium state, including the tube's confinement ($\chi = D/D_{rbc}$), the flow rate, and the cells' starting location. However, there is a lack of comprehensive research on how these variables affect the equilibrium state transition. Additionally, most previous studies on cell equilibrium states in circular tubes ignored the effect of initial location, and it is uncertain if the "bistability" phenomena [1] observed in rectangular tubes persists in axisymmetric Poiseuille flow in a cylindrical microchannel. The distribution pattern of cells' equilibrium states under high shear rates (up to $1000s^{-1}$) requires further investigation to meet the need for high throughput separation of rare cells in microfluidic chips.

In this report, We presented a comprehensive analysis of the effects of flow characteristics on the equilibrium state of erythrocytes in circular microchannels. The cells were initially positioned at various radial locations in order to study how their starting conditions affected their equilibrium states. In compared to prior investigations, the present simulations took a greater range of shear rates($\bar{\dot{\gamma}} = \bar{U}/D: 5\sim1000s^{-1}$) into account. And this knowledge may aid in the development of microfluidic devices for isolating rare cells and assessing cell deformability at a high throughput.

## 2. Specific usage status of the system and calculation method

In FY2021, our Quick Use project used about 3,000,000 core*hours. A parallel software based on OpenMP and MPI was used to simulate the motion and deformation of red blood cells in a constrained microchannel.

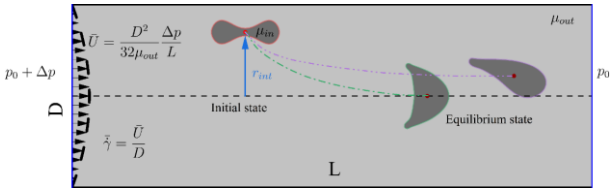


Fig. 1. Schematic diagram of the boundary conditions of the present simulation.

The dynamic problem of a single deformable RBC suspended in an incompressible Newtonian fluid in a three-dimensional circular microchannel is investigated. The fluid-structure interaction(FSI) problems are solved by the immersed boundary method(IBM) [2]. In the computational domain

shown in Figure 1, the motion of fluid inside and outside the RBCs is governed by the Navier-Stokes equation:

$$\nabla \cdot \mathbf{u} = 0, \tag{1}$$

$$\rho\left(\frac{\partial \mathbf{u}}{\partial t} + \mathbf{u} \cdot \nabla \mathbf{u}\right) = -\nabla p + \nabla \cdot \mu(\nabla \mathbf{u} + \nabla \mathbf{u}^T) + \mathbf{f} \tag{2}$$

where $\rho$,$\mathbf{u}$,$t$,$p$ and $\mu$ are the fluid density, velocity vector, time, pressure and viscosity, respectively. The no-slip condition is satisfied in the flow field around the cell membrane, and the velocity of the Lagrangian grid is determined by integrating the velocity of the surrounding Eulerian grid with Dirac $\delta$ function

$$\frac{\partial \mathbf{X}}{\partial t} = \mathbf{U}(\mathbf{X}, t) = \int_{\Omega} \mathbf{u}(\mathbf{x}, t)\delta_3(\mathbf{x} - \mathbf{X})\mathrm{d}\mathbf{x}, \tag{3}$$

where $\mathbf{x}$ and $\mathbf{X}$ are the arbitrary Eulerian mesh in the computational domain and Lagrangian grid on the membrane, respectively. $\delta_3(\mathbf{x} - \mathbf{X})$ is a three-dimensional smoothed delta function, can be found in Peskin's work[2]. The last term in equation (2) is the source term for FSI problems in the IBM, $\mathbf{f}$ represents the smoothed force exerted by the RBC membrane which is calculated as

$$\mathbf{f}(\mathbf{x}) = \int_{\Gamma} \mathbf{F}(\mathbf{X}, t)\delta(\mathbf{x} - \mathbf{X})\mathrm{dS}(\mathbf{X}), \tag{4}$$

where $\mathbf{F}(\mathbf{X},t)$ indicates the local stress density on the membrane. Elastic forces arising from membrane deformation, which include resistance to shearing deformation, area dilation, and out-of-plane bending, balance the force exerted by the fluid on the cell membrane. The shearing deformation and area dilation are governed by Skalak's law,

$$W_s^{SK} = \frac{E_s}{4}\left(\frac{1}{2}I_1^2 + I_1 - I_2 + \frac{1}{2}CI_2^2\right), \tag{5}$$

where $G_s$ is the membrane shear modulus, $C$ is the dimensionless dilation ratio. $I_1 = \lambda_1^2 + \lambda_2^2 - 2$ , $I_2 = \lambda_1^2\lambda_2^2 - 1$ are the strain invariants of the left Cauchy-Green surface deformation tensor $\mathbf{B}$, and $\lambda_1$ and $\lambda_2$ are the principal stretch ratio of the local membrane. The principle tension $\tau_1$ and $\tau_2(\tau_1 \geq \tau_2)$ on the membrane is obtained as

$$\tau_1 = \frac{1}{\lambda_2}\frac{\partial W_s}{\partial \lambda_1} = \frac{G_s\lambda_1}{\lambda_2}[\lambda_1^2 - 1 + C\lambda_2^2(\lambda_1^2\lambda_2^2 - 1)], \text{(likewise for } \tau_2\text{)}. \tag{6}$$

More details about calculation of membrane in-plane tension can be found in Gong et al. [3,4] and Le et al.[5]. The bending force on the membrane was modeled with the linear bending model [5], the bending moment can be calculated as

$$\mathbf{m} = E_b(\boldsymbol{\kappa} - H_0\mathbf{P}), \tag{7}$$

where $E_b$ is the bending rigidity, $\mathbf{P} = \mathbf{I} - \mathbf{nn}$ is the tangential projection operator, $\mathbf{n}$ is the unit normal vector, $\boldsymbol{\kappa}$ is the local curvature tensor of deformed membrane and $H_0$ is the mean curvatures of the resting configurations. Following the process of Le et al.[5], the transverse shear tension is obtained by

$$\mathbf{q} = \nabla_s \cdot \mathbf{m} \cdot \mathbf{P}, \tag{8}$$

where surface gradient operator $\nabla_s = \mathbf{P} \cdot \nabla$. Then the elastic force $\mathbf{F}_e$ and bending force $\mathbf{F}_b$ on the Lagrangian mesh points can be calculated as

$$\mathbf{F}_e = \nabla_s \cdot \boldsymbol{\tau}, \tag{9}$$

$$\mathbf{F}_b = \nabla_s \cdot (\mathbf{qn}). \tag{10}$$

In addition, an extra penalty volume force $\mathbf{F}_V$[6] is introduced to suppress the unavoidable artificial volume drift [1] of the cell,

$$\mathbf{F}_V = -C_V\frac{V - V_0}{V_0}\mathbf{n}, \tag{11}$$

where $C_V$ is the penalty coefficient, $V_0$ and $V$ is the are the cell volumes at the initial and current moments, respectively.

Combined above equations, the membrane force in equation (4) can be obtained by

$$\mathbf{F} = \mathbf{F}_e + \mathbf{F}_b + \mathbf{F}_V. \tag{12}$$

The membrane force is solved by finite element method. The icosahedron grid is utilized to produce the Lagrangian mesh by mapping and segmentation in order to create an isotropic and homogenous mesh on the cell membrane. More details can be found in Le et al. [5].

To investigate the effect of the difference in viscosity between inside and outside the cell, we introduce the Indicator function $I(\mathbf{x},t)$

$$I(\mathbf{x},t)\begin{cases}=1, & \mathbf{x}\ in\ the\ interior\ of\ a\ cell\\ \in(0,1), & \mathbf{x}\ in\ the\ neighborhood\ of\ interface\\ =0, & \mathbf{x}\ outside\ a\ cell\end{cases} \quad (13)$$

The distribution of the viscosity in the computational domain can be defined with the indicator function as

$$\mu(\mathbf{x},t)=\mu_{out}+(\mu_{in}-\mu_{out})I(\mathbf{x},t) \quad (14)$$

where the indicator function $I(\mathbf{x},t)$ is obtained by solving the following Poisson equation

$$\nabla^2 I(\mathbf{x},t)=\nabla\cdot\mathbf{G}(\mathbf{x},t), \quad (15)$$

where

$$\mathbf{G}(\mathbf{x},t)=\int_\Gamma \mathbf{n}(\mathbf{X},t)\delta_3(\mathbf{x}-\mathbf{X})\mathrm{d}S(\mathbf{X}). \quad (16)$$

The Navier-Stokes equations (Eqs. (1)&(2) ) are solved with the Simplified Marker and Cell(SMAC) Method. The computations are done on a staggered grid using second-order central discretization for the spatial discretization; implicit Euler scheme is used for viscous term to loosen timestep constraints. more details about the algorithm can be found in Gong et al. [3,4] and Wang et al.[6].

For more information about the values of the computational parameters and the validation of the numerical techniques, please consult our upcoming publication.

## 3. Result

In this work, we numerically investigate the dynamic behavior of a single RBC in a 3D circular microchannel with varying flow rates $\dot{\gamma}$, and the RBC is released from various radial positions $r_{int}$ to explore the impact of the initial location on the equilibrium state. The equilibrium state of a cell is characterized as one in which its morphology and radial position remain constant or shift periodically. Numerical experiments revealed that when the shear rate $\dot{\gamma}$, and the initial position $r_{int}$ vary, the cell enters one of four equilibrium states.


Fig 2. The four equilibrium states of RBC varies with different shear rates. (a)$\bar{\dot{\gamma}} = 2s^{-1}$, RBC in “snaking” state; (b) $\bar{\dot{\gamma}} = 20s^{-1}$, RBC in “tumbling” state; (c) $\dot{\gamma}^* = 50s^{-1}$, RBC in "parachute" state; (d) $\dot{\gamma} = 160s^{-1}$,RBC in "slipper" state.

From top to bottom, Figure 2 displays the "snaking," "tumbling," "parachute," and "slipper" motions of erythrocytes with varying shear rates in a microchannel with a diameter $D = 14\mu m$. The cells were initially positioned $1.5\mu m$ from the tube's center.

The numerical results reveal that when the shear rate is low enough($\sim 1s^{-1}$), erythrocytes move in a "snaking" pattern around the tube center with negligible cell deformation, as shown in Fig 2(a). As the flow rate increases, the cell approaches equilibrium in a periodic "tumbling" motion at a given off-center location, as shown in Fig 2(b). With increasing shear rate, the cell loses its biconcave disc-like shape and most often resembles a "slipper" (see Fig. 2-2(d)). Owing to the increased shear stress, the cell membrane is in a tank-treading motion, which is interspersed with periodic "tumbling" due to the difference in internal and exterior viscosity. When the shear rate reaches a certain level (~50 $s^{-1}$), the cells are in a "parachute" (as in Figure 2-2(c)), or "Croissant"[1] motion near the tube center. Despite the fact that the RBC shape has stabilized, the Lagrangian point on the cell membrane continues to wander on the cell surface.

To quantitatively characterize the motion of

various equilibrium states, this paper refers to the work of Fedosov et al. [7] and introduces three dimensionless parameters:

(1) To simplify, we establish a Cartesian coordinate at the channel's centerline and align the flow direction with the x-axis. The distance of the cell center of mass from the tube centerline can be defined as

$$d_{mc}(t) = \|(\mathbf{I} - \mathbf{e}_x\mathbf{e}_x) \cdot \mathbf{X}_{mc}\|, \quad (17)$$

in which $\mathbf{e}_x$ is the unit vector in the flow direction, $\mathbf{X}_{mc}$ is the location of the mass center of the cell, defined as

$$\mathbf{X}_{mc}(t) = \frac{\sum_{i=1}^{N}\mathbf{X}_i(t)}{N}, \quad (18)$$

where N is the total number of Lagrangian points on the cell membrane, and $\mathbf{X}_i(t) = (X_i(t), Y_i(t), Z_i(t))$ is the position of the i-th point on the membrane at time t. The variation of $d_{mc}(t)$ with time is shown in Figure 3(a).

(2) The asphericity characterizes the deviation of cell shape from spherical shape. With the help of the gyration tensor

$$\mathbf{G}(t) = \frac{1}{N}\sum_{i=1}^{N}(\mathbf{X}_i(t) - \mathbf{X}_{mc}(t))\otimes(\mathbf{X}_i(t) - \mathbf{X}_{mc}(t)) \quad (19)$$

The asphericity can be defined as

$$\alpha_{asphe} = \frac{(\lambda_1-\lambda_2)^2+(\lambda_1-\lambda_3)^2+(\lambda_2-\lambda_3)^2}{2(\lambda_1+\lambda_2+\lambda_3)^2}, \quad (20)$$

where $\lambda_1$、$\lambda_2$、$\lambda_3$ are the three eigenvalues of $\mathbf{G}(t)$. When the cell is in the stress-free state, its asphericity is 0.15, and Figure 3(b) shows the variation of asphericity with time for different motion states.

(3) Assuming that $\lambda_1 \geq \lambda_2 \geq \lambda_3$,the corresponding eigenvectors are $\mathbf{e}_1$、$\mathbf{e}_2$、$\mathbf{e}_3$, then the cell orientation angle is obtained as follows

$$\theta = \arccos(\mathbf{e}_3 \cdot \mathbf{e}_x), \quad (21)$$

The orientation angle can be defined as the angle between orientation axis $\mathbf{e}_3$ and the flow direction $\mathbf{e}_x$, which can be considered as the angle between the rotational axis of erythrocytes and the direction of flow (as shown in Figure 3(c)), and the time history of the orientation angle is presented in Figure 3(d).

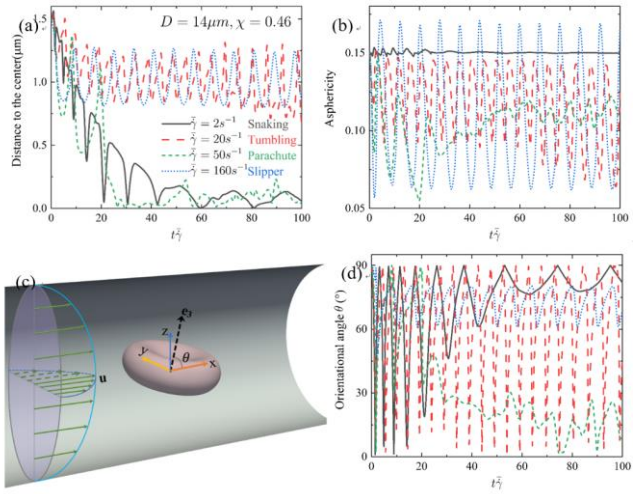


Fig 3, The time history of cell centroid position, asphericity, and orientation angle of cells under various equilibrium states. Different colors represent different equilibrium states. (a) Centroid position; (b) Asphericity; (c) Schematic diagram of orientation angle; (d) Orientation angle.

Figure 3 illustrates the dynamical characteristics of various motion of RBCs affected by different shear rates. "Snaking" erythrocytes are near the center of tube, with negligible deformation, and their orientation angle varies periodically between about 75 and 90 degrees. In contrast, the "Parachute" red blood cells also situate in the center exhibits a much larger deformation and have an azimuth angle of less than 30 degrees. "Slipper" and "Tumbling" erythrocytes show similar dynamic behavior, with equilibrium deviating from tube center and asphericity oscillating periodically over a wide range. As mentioned, the primary difference between the two is that in a “Tumbling” motion, the erythrocyte orientation angle is completely flipped, whereas in a “Slipper” condition it oscillates within a narrow range (usually no more than 20 degrees). Quantifying the above dimensionless

parameters allows for a clear understanding of the equilibrium state of erythrocytes under various flow conditions.

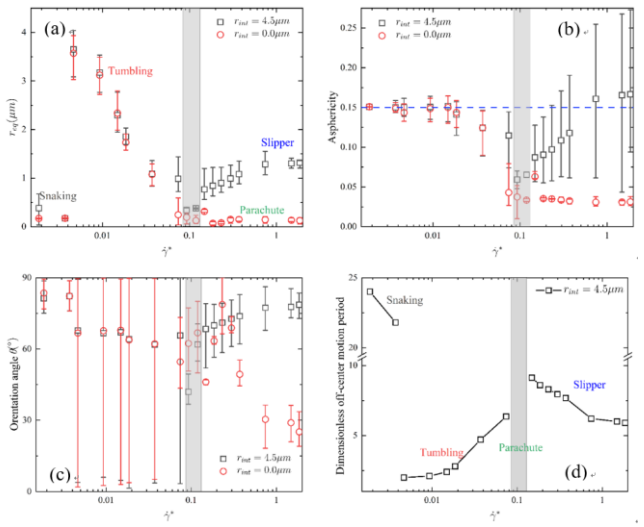


Fig 4. The effect of initial position on cell equilibrium state and dynamic behaviors under different shear rates. (a) Equilibrium position $r_{eq}$; (b) Asphericity $\alpha_{asphe}$; (c) Orientation angle $\theta$; (d) Dimensionless period of motion after reaching steady state, which is nondimensionalized with $\bar{\dot{\gamma}}$.

Further numerical experiments revealed that the equilibrium state of the cell is not only influenced by the shear rate but also by the initial position of the cell. Figure 4 demonstrates the combined effect of initial position and shear rate on the stable morphology of the cells, with black boxes in the figure representing cells initially placed near the tube wall and red circles representing cells initially positioned in the center of the tube. In the figure the horizontal axis represents the dimensionless shear rate, whereas the vertical axes from Fig 4(a) to Fig4(d) indicate the average value of each dynamic parameter when the cell has reached steady state, with the upper and lower bars representing the corresponding maximum and minimum values.

As shown in Fig 4, as the dimensionless shear rate increases, the cell transitions from "Snaking" to "Tumbling", then "Parachute", at last "Slipper" or "Parachute", depending on the initial position:

i) In the case where the shear rate is very low($\dot{\gamma}^* < 0.003$), the cell shows a "snaking" motion near the tube center regardless of its initial position. Due to the very low shear rate, the cells undergo little deformation and the cyclic motion has an exceptionally long period.

ii) With a shear rate $\dot{\gamma}^*$ between 0.003 and 0.08, the equilibrium state of the cell is in the "tumbling" state near the tube wall. As the shear rate increases, the erythrocytes' equilibrium position in the tumbling motion moves closer to the tube center, the motion period lengthens, and the deformation amplitude increases.

iii) As the shear rate $\dot{\gamma}^*$ approaches 0.1 (gray shaded region in the Fig 4), the equilibrium state takes the shape of a "parachute," regardless of an initial position for the cell.

iv) When the shear rate $\dot{\gamma}^*$ is greater than 0.15, the equilibrium state of erythrocytes is bistable[1] depending on the initial position: Cells initially located in the tube center end up in a "Parachute" motion, whereas cells initially located in the tube's periphery end up in a "Slipper" motion. Additionally, when the shear rate increases, the equilibrium location of the red blood cells in the "slipper" motion migrated farther from the tube's center, with larger deformation and shorter motion cycles.

We plotted the phase diagram of the cell's equilibrium state in order to illustrate the combined effect of shear rate and initial position. Fig. 5 illustrates numerical results of RBCs in microchannel with tube diameters of 14 $\mu m$. The horizontal axis represents the dimensionless shear rate whereas the vertical axis represents the dimensionless initial position, and each points represents a cell in a different state of motion.

The findings indicate that for low shear rates ($\dot{\gamma}^* < 0.08$ or $\dot{\gamma}^{**} < 80$), the initial position has no influence on the equilibrium state. The

equilibrium state of cells undergoes a change from "snaking" to "tumbling" and finally to "parachute" with increasing shear rate, which is consistent with the results of Fedosov et al. [7]. With a shear rate $\dot{\gamma}^*$ of roughly $0.1(\dot{\gamma}^{**}\sim100)$, independent of the starting position, the equilibrium state of RBCs is a "parachute" motion in the tube's center, which is consistent with prior results in square channels[1,8]. The equilibrium state of cells at high shear rates $(\dot{\gamma}^* > 0.2 \text{ or } \dot{\gamma}^{**} > 200)$ is affected by the initial position: cells with initial positions close to the tube center become "parachutes", while cells with initial positions close to the wall become "slippers", and the critical initial position that determines this “bistability” phenomenon tends toward the center of the tube as the shear rate increases.

Previous study also observed similar bistability phenomena of "parachute" and "slipper" motions. Agarwal et al. [9] discovered that in the absence of a strong tube wall confinement, the presence of an internal and external viscosity difference may induce this bistability phenomenon. Tahiri et al. [8] and Guckenberger et al. [1] observed "slipper" and "parachute" coexistence phenomenon in rectangular channels, but did not specify whether this is due to the square tube flow's asymmetry. Our study of RBC motion in 3D circular channels shows that the initial position-dependent bistability persists even in completely axisymmetric flows, which is impacted by the shear rate.

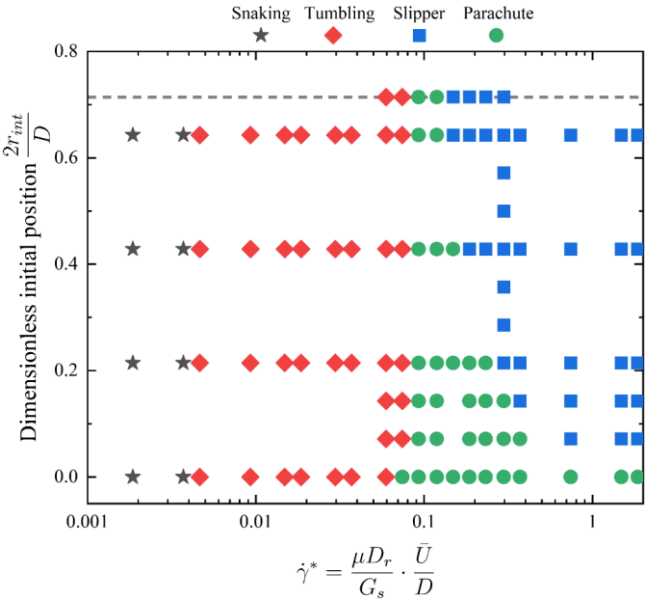


Fig 5. The phase diagram of different state in the parameter space of initial position $2r_{int}/D$ and dimensionless shear rate $\dot{\gamma}^*$. The diameter of microchannel is $14\mu m$. Numerous colored and shaped points represent distinct stable states: "Snaking" is represented by the black pentagram, "Tumbling" is represented by the red diamond, "Parachute" is represented by the green circle, the blue box represents the "Slipper" motion. The dashed line in the figure represents the farthest initial position that the cell can be placed.

## 4. Conclusion

The equilibrium state and dynamic behavior of a single red blood cell in a circular tube were studied. It was discovered that when the shear rate rises, the equilibrium state of a single erythrocyte changes from "snaking," "tumbling," "slipper," to "parachute"; under the effect of high shear rate, the equilibrium state is either "slipper" or "parachute," depending on the cell's initial position. The phase diagram was obtained by performing a systematic analysis of the equilibrium state under the impact of the initial location of RBC and shear rate.

Our simulation results show that the effect of the initial position on the equilibrium state varies with the shear rate when multiple lift forces are simultaneously applied. For the low shear rates$(\dot{\gamma}^* < 0.1)$, the initial position of RBCs does

not influence the equilibrium state, and as the shear rate increases, equilibrium state changes from "Snaking" to "Tumbling" and then to “Parachute”, which is consistent with previous observations. When flow rate increased, the equilibrium position of the cells moves toward the center of the pipe mainly due to Magnus lift force and deformation-induced lift force. When the shear force is significant, the RBC is subjected to both inertial lift force and deformation-induced lift force, and the equilibrium state is either a "Parachute" near the center or a "Slipper" away from it, depending on its initial location. Furthermore, as the diameter of the tube increases and the wall confinement decreases, the cell equilibrium state is likely to be off-center "Tumbling" or "Slipper" and the equilibrium position moves farther and farther away from the tube center. Microfluidic chips for isolating rare cells may be developed in the future based on the complicated effects of shear rate and initial position on the equilibrium position of erythrocytes that we observed.

## 5. Schedule and prospect for the future

A numerical analysis has been conducted on the equilibrium state of RBCs in cellular scale in three-dimensional straight circular tubes or tubes and the equilibrium state of RBCs with different initial positions has been obtained under various flow conditions. However, it remains unclear how erythrocytes in different states of motion affect their mass transfer efficiency in the microcirculation.

As a next step, we would like to examine, on the basis of the present numerical results, the differences in the stress distribution of the cell membranes in different states and the effect of these differences on processes such as gas exchange[4,6] and ATP release. We hope that RIKEN will continue to provide sufficient computational resources in the coming fiscal year to assist us in investigating the mechanisms of mass transfer across RBC membrane under the influence of complex flow conditions, and that our findings will contribute to a better understanding of some metabolic diseases such as Alzheimer's disease.

## Reference

[1] Guckenberger A, Kihm A, John T, Wagner C, Gekle S. Numerical–experimental observation of shape bistability of red blood cells flowing in a microchannel. Soft Matter. 2018;14(11):2032-43.

[2] Peskin CS. The immersed boundary method. Acta numerica. 2002 Jan;11:479-517.

[3] Gong X, Sugiyama K, Takagi S, Matsumoto Y. The deformation behavior of multiple red blood cells in a capillary vessel.

[4] Gong X, Gong Z, Huang H. An immersed boundary method for mass transfer across permeable moving interfaces. Journal of Computational Physics. 2014 Dec 1;278:148-68.

[5] Le DV, White J, Peraire J, Lim KM, Khoo BC. An implicit immersed boundary method for three-dimensional fluid–membrane interactions. Journal of computational physics. 2009 Dec 1;228(22):8427-45.

[6] Wang X, Gong X, Sugiyama K, Takagi S, Huang H. An immersed boundary method for mass transfer through porous biomembranes under large deformations. Journal of Computational Physics. 2020 Jul 15;413:109444.

[7]Fedosov DA, Peltomäki M, Gompper G. Deformation and dynamics of red blood cells in flow through cylindrical microchannels. Soft matter. 2014;10(24):4258-67.

[8] Tahiri N, Biben T, Ez-Zahraouy H, Benyoussef A, Misbah C. On the problem of slipper shapes of red blood cells in the microvasculature. Microvascular research. 2013 Jan 1;85:40-5.

[9] Agarwal D, Biros G. Stable shapes of three-dimensional vesicles in unconfined and confined Poiseuille flow. Physical Review Fluids. 2020 Jan 28;5(1):013603.

**Fiscal Year 2021 List of Publications Resulting from the Use of the supercomputer**

**[Paper accepted by a journal]**

**[Conference Proceedings]**

**[Oral presentation]**

**[Poster presentation]**

1. **Xiaolong Wang**, Peng Jing, Qiaodong Wei, Shenghong Zhang and Xiaobo Gong. *An Immersed Boundary Method for Mass Transfer through Porous Biomembranes under Large Deformations*. Poster presented at: the 16th IEEE International Conference on Nano/Micro Engineered & Molecular Systems (IEEE-NEMS 2021); 2021 Apr 25-29; XiaMeng, China.
2. De-Yun Liu, Peng Jing, **Xiaolong Wang**, Qiaodong Wei, Shenghong Zhang and Xiaobo Gong. *A Numerical Study on the Effects of Mechanical Properties of Red Blood Cells on Rheology in Narrow Microchannels*. Poster presented at: the 16th IEEE International Conference on Nano/Micro Engineered & Molecular Systems (IEEE-NEMS 2021); 2021 Apr 25-29; XiaMeng, China.

**[Others (Book, Press release, etc.)]**